J Sol-Gel Sci Technol (2008) 47:173–181
DOI 10.1007/s10971-008-1784-2

ORIGINAL PAPER

Polyvinylpyrrolidone/ZrO_2-based sol–gel films applied in highly reflective mirrors for inertial confinement fusion

Liping Liang · Yao Xu · Lei Zhang · Dong Wu · Yuhan Sun

Received: 16 November 2007 / Accepted: 29 May 2008 / Published online: 16 June 2008

Abstract Polyvinylpyrrolidone (PVP)/ZrO_2-based hybrid thin films, with suitable properties for application in the high power lasers, have been prepared combining the advantages of both the sol–gel route and the organic-inorganic hybrid materials. By virtue of light scattering analysis, the chemical composition of the reaction system was fully optimized, endowing the films with good optical properties and high laser-induced damage threshold (LIDT). Light scattering studies also provided valuable structural information about the hybrid sols, which offered a better understanding of the structure and performance of the hybrid films. Our experiments showed that, in the hybrid sols, the incomplete substitution for the chelating ligands by the hydroxyls might considerably conceal and weaken the effect of PVP on the nucleation and growth of ZrO_2 particles. Thus, the incorporation of PVP only resulted in slight decreases in the refractive index and LIDT of the films. By energy relaxation through their flexible polymer chains, however, the addition of PVP could easily enhance the stress compatibility between the high- and low-index layers and then facilitate the deposition of the multi-layer highly reflective mirrors.

Keywords Zirconia · Sol–gel · Optical coatings · Light scattering

L. Liang · Y. Xu (✉) · L. Zhang · D. Wu · Y. Sun
State Key Laboratory of Coal Conversion, Institute of Coal Chemistry, Chinese Academy of Sciences, Taiyuan 030001, China
e-mail: xuyao@sxicc.ac.cn

L. Liang
College of Material Science and Engineering, Taiyuan University of Science and Technology, Taiyuan 030024, China

1 Introduction

The potential application of high-power lasers as the ignition source of inertial confinement fusion (ICF) has stimulated the research and development of various laser optical components such as the anti-reflective (AR) mirrors, highly reflective (HR) mirrors, polarizer, and so forth. Among them, the fabrication of the HR mirrors is a real challenge and has been an area of considerable interest in recent years [1–11]. For HR mirrors working at a given wavelength, λ_0, the preparation involves an alternate deposition of high- and low-refractive index layers, each with an optical thickness equal to one-quarter of λ_0. The reflectivity of the HR mirrors increases with the increase in either the number of stacked pairs or refractive index contrast between two materials [12]. Unfortunately, two layers of highly different refractive index usually present different internal stresses due to their different natures and structures. This may induce interfacial stresses often expressed by film cracking or delaminating. Moreover, to obtain the best optical performance, any defaults such as impurities, structural defects and low surface homogeneity must be excluded [8, 13, 14]. Hence, to assemble the HR mirrors, it is of great importance to precisely control the structure and property of every monolayer in the film stacks.

Such a precise control on the structure and performance of films can only be achieved by the proper selection of both the material and deposition process. Among the widely examined materials for HR mirrors, ZrO_2 and SiO_2 have proved to be a pair of potential candidates for the high- and low-index film materials, due to their good optical properties and high chemical and thermal stabilities [1–18]. As concerning the film depositions, a variety of physical and chemical techniques have been developed,

among which the soft sol–gel route is more attractive. Firstly, the porous sol–gel films tend to be more favorable to energy relaxation through their network structure, thus endowing films with low internal stress and high laser-induced damage resistance [1–10, 15]. Secondly, the sol–gel route offers an excellent control on the composition, purity, and homogeneity of films. This greatly diminishes the probability of default formation in the films [1–11, 13, 14]. Finally, such a process gives advantages to produce the organic–inorganic (O/I) hybrid materials, which provides another way to alleviate the film stress, and then facilitates the fabrication of the multi-layer mirrors [10, 19–22].

Sol–gel deposition of SiO_2- and ZrO_2-based films has been extensively studied. As one of the most widely studied AR films, the sol–gel deposition techniques for SiO_2 films have been established [1–10, 15], and the involved sol–gel chemistry has been primarily elucidated [23, 24]. In comparison, progresses in the sol–gel deposition of ZrO_2 high-index layers are rather slow, which greatly restricts the development of sol–gel HR mirrors. Many researches demonstrated that the bottleneck consists in the synthesis of ZrO_2 precursor sols [3–7, 9, 10, 25]. By far, two types of approaches have been developed to prepare ZrO_2-based sols. One is the suspension route, which involves the formation of nanocrystalline particles by a hydrothermal process and then a subsequent redispersion of the particles in alcohol solvent to produce suitable suspensions for film deposition. In this area, many precursory and excellent works should be attributed to the efforts of Thomas [1, 3], Floch et al. [2], and Belleville et al. [5, 10]. The other is the chelating route, which produces sols directly based on the controlled hydrolysis-condensation of zirconium alkoxides [4, 6, 26–30]. With no need of further redispersion, the chelating route offers more conveniences in synthesizing homogeneous sols and then high-performance optical films. The feasibility of the chelating route in depositing the high-index layer of HR mirrors has been demonstrated by McInnes et al. [4, 6].

The chelating route, just as its name implies, is such one, in which the hydrolysis and condensation of zirconium alkoxides is chemically controlled by modifying the precursors with chelating ligands to produce new molecular species with altered structure and reactivity. So far, a variety of chelators, such as organic acids [25, 26], hydroxyketone, alkanolamines [27], diketones [28, 29], and glycols [30], have been developed. Based on these chelators, ZrO_2 films for various common applications have also been successfully deposited [26, 31, 32]. Unfortunately, in most researches, strong chelators in excessive amounts are often employed to ensure enough stability of the sols [27–30], which makes the films unable to acquire their necessary properties until undergoing a heat-treating process. However, such a post treatment is impracticable for the multi-layer mirror deposition, since heat-treating the film stacks, even at a medium temperature, may induce considerable thermal stress and lead to film cracking or delaminating [1–10]. In other words, for application in HR mirrors, ZrO_2 films must acquire their properties immediately after the deposition, which requires a good balance between the chelation and hydrolysis-condensation in the colloidal system so as to produce sols with sufficient hydrolysis of zirconium and proper stability. This is beyond the scope of the current researches on the chelating sol–gel route for ZrO_2 materials. Moreover, although the decisive effects of the precursor sols on the structure and properties of films have been recognized, little research has been done involving the correlation between sol structures and properties of its xerogel films.

The aim of our present work was to produce polyvinylpyrrolidone (PVP)/ZrO_2-based hybrid films, combining the advantages of both the sol–gel route and O/I hybrid materials, and examine their properties for use as the high-index layer in HR mirrors at 1,064 nm. With diethanolamine as the chelating agent, PVP/ZrO_2-based hybrid sols and films were prepared via the chelating sol–gel route and spin-coating process. The sols were studied by the light scattering techniques to obtain necessary structural information. The chemical composition, structural properties and optical performances of these films were characterized. Based on these analyses, a possible correlation between the film properties and microstructure of the precursor sols was also presented.

2 Experimental

2.1 Preparation of sols and films

All chemicals, including Zirconium (IV) *n*-propoxide ($Zr(OPr)_4$, Strem chemicals), PVP (K85–95, mean molecular weight of 1,300,000, Acros chemicals), diethanolamine (DEA, Tianjin chemicals), Tetraethoxysilane (TEOS, Acros chemicals), ammonia ($NH_3{\cdot}H_2O$) and anhydrous ethanol (Beijing chemicals), were of reagent grade and used without further purification.

The entire procedure, including the sol preparation and film deposition, was carried out in a clean and controlled atmosphere with the temperature of 20 °C and relative humidity of 45%.

During the synthesis of PVP/ZrO_2-based sols, two different parts of alcohol solutions were prepared. In the first part, the deionized water and PVP were dissolved into anhydrous ethanol by stirring under the sealed conditions. The second part of solution was then prepared by dissolving $Zr(OPr)_4$ in anhydrous ethanol containing DEA. The

solution was sealed and kept stirring for 30 min to achieve a complete chelation between $Zr(OPr)_4$ and DEA. Hydrolysis and condensation was then carried out by rapid mixing the two solutions by vigorous stirring, which led to the formation of fresh sol. The initial concentration of $Zr(OPr)_4$ in the total mixture, C, was 0.28 mol/L. The molar ratio of H_2O and $Zr(OPr)_4$ (namely hydrolysis ratio, r) was 2:1. The molar ratio of DEA and $Zr(OPr)_4$ (namely chelating ratio, d) and the mass fraction of PVP in the total amount of PVP and the converted ZrO_2, W_{PVP}, were varied as shown in Table 1. The designed concentration of ZrO_2 in the final sol was 4.3 wt%. All fresh sols were hermetically stirred for 60 min and held under static conditions for 20-day aging to obtain the precursor sols for film deposition.

For HR mirror preparation, SiO_2 sol was prepared by the ammonia-catalyzed hydrolysis and condensation of TEOS in ethanol according to Stöber's method [23]. The concentration of TEOS in total mixture, C, was 0.58 mol/L, the hydrolysis ratio, r, was 2:1, and the molar ratio of NH_3 and TEOS (namely catalysis ratio, c) was 1.75×10^{-4}:1. The designed concentration of SiO_2 was 4.4 wt%. The fresh sol was aged for 15 days to obtain the precursor sols for film deposition.

PVP/ZrO_2-based and SiO_2 single-layer coatings were prepared by spin coating the aged precursor sols onto the well-cleaned K9 optical glass substrate. To obtain films with the optical thickness of one-quarter of 1,064 nm, the deposition speed was precisely controlled. For PVP/ZrO_2-based sols, the spinning rate of the substrate was changed from 1,800 to 3,500 rpm. For SiO_2 sol, the spinning rate was fixed at 2,100 rpm. The fabrication of the HR mirrors involved an alternate deposition of PVP/ZrO_2-based and SiO_2 quarter-wave films. During deposition, each fresh layer was air-dried for 20 min under the continuously spinning conditions at 2,000 rpm before the next layer was deposited.

To simplify discussion, ZrO_2-based sols, PVP/ZrO_2-based sols, PVP/ZrO_2-based films, and the HR mirrors were named hereafter "SZX, SZPY, FZPY, and HRY", where S, F, and HR respectively denoted the sols, films, and HR mirrors, X was the value of chelating ratio, d, in ZrO_2-based sols, and Y indicated the mass fraction of PVP in PVP/ZrO_2-based hybrid sols and the high-index films.

2.2 Characterization of sols and films

To obtain necessary structural information, the precursor sols used for film deposition were examined using the small-angle X-ray scattering (SAXS) and dynamic light scattering (DLS) techniques. The SAXS experiments were carried out with a long-slit collimation system on 4B9A beamline at Beijing Synchrotron Radiation Facility, China. The incident X-ray wavelength, λ, was 0.154 nm, the scattering angle, 2θ, was 0–3°, and the scattering vector,

Table 1 Composition and structural parameters of ZrO_2-based, PVP/ZrO_2-based and SiO_2 colloid system[a]

Sample	Composition				Stable sol*	Mean particle size			η (cP)
	C (mol L^{-1})	r	d or c	W_{PVP} (%)		$D_{m,SAXS}$ (nm)	$D_{h,DLS}$ (nm)		
SZ2.0	0.28	2:1	2.0:1	0	Yes	–	–	–	–
SZ1.5	0.28	2:1	1.5:1	0	Yes	–	–	–	–
SZ1.0	0.28	2:1	1.0:1	0	Yes	1.3	3.7	19.8	–
SZ0.8	0.28	2:1	0.8:1	0	Yes	3.3	5.2	20.4	–
SZ0.7	0.28	2:1	0.7:1	0	Yes	3.5	5.7	25.2	–
SZ0.6	0.28	2:1	0.6:1	0	Yes	3.9	6.1	27.5	1.76
SZ0.5	0.28	2:1	0.5:1	0	No	4.1	6.7	35.4	–
SZP00	0.28	2:1	0.6:1	0	Yes	3.9	6.1	27.5	1.76
SZP05	0.28	2:1	0.6:1	5	Yes	4.0	6.1	20.7	1.91
SZP10	0.28	2:1	0.6:1	10	Yes	3.9	6.5	27.6	2.27
SZP15	0.28	2:1	0.6:1	15	Yes	4.0	6.7	28.5	2.63
SZP20	0.28	2:1	0.6:1	20	Yes	3.8	6.2	21.8	3.08
SiO_2 sol	0.58	2:1	1.75e-4:1	0	Yes	–	12.3		1.82

[a] The upper error limit for all the derived values is within 5%

C is the initial concentration of $Zr(OPr)_4$ or TEOS in the reaction system. r is the hydrolysis ratio, being defined as the molar ratio of H_2O and $Zr(OPr)_4$ (or TEOS). d is for ZrO_2-based sols and denotes the molar ration of DEA and $Zr(OPr)_4$. c is for SiO_2 sol and denotes the molar ratio of NH_3 and TEOS. W_{PVP} is the mass fraction of PVP in the total amount of PVP and the converted ZrO_2. *A stable sol refers to the system that can maintain transparent state and good fluidity after 20-day aging (for ZrO_2-based sols) or 15-day aging (for SiO_2 sol) at 293 K. $D_{m,SAXS}$ is the mean diameter of the colloidal particles derived from SAXS, and $D_{h,DLS}$ is the hydrodynamic diameter measured by DLS. η is the viscosity of sol examined at a rotor-spinning rate of 100 rpm

$q = 4\pi\sin\theta/\lambda$. The background scattering was corrected to obtain the $J(q) - q$ curves, $J(q)$ being the scattering intensity. The size distribution of the scatterers was determined using Shull-Roess method [33]. And their fractal characteristics were determined directly based on the power law regions in $J(q) - q$ curves according to the method reported by Keefer et al. [34] and McMahon et al. [35]. The DLS analysis was performed on a particle size analyzer (Coulter, N4Plus) with a He–Ne laser. The scattered light was detected simultaneously at two scattering angles of 29.1° and 90°. Scattering data from each angle were analyzed independently to obtain the particle size distribution curves. The viscosity of several sols was examined on a rheometer (Brookfield, LV DV-III+) at a rotor-spinning rate of 100 rpm. Both the light scattering experiments and viscosity analysis were performed at a constant temperature of 293 K.

Fourier Transform Infrared (FTIR) spectra were recorded on a FTIR spectrometer (Nicolet, Magna-II 550). For FTIR analysis, the film samples were specially prepared by spin coating the sols directly onto the KBr flakes. The atomic force microscope (AFM, Digital Instrument, Model DI 5000) was used to probe the surface morphology of the films. The transmission spectra were measured using an ultraviolet/visible/near infrared (UV/Vis/NIR) spectrometer (Perkin–Elmer, Lambda-900). The films were further examined by a high-resolution thin-film metrology system (SCI, FilmTek^{TM}3000) to determine the refractive index, $n(\lambda)$, extinction coefficient, $k(\lambda)$, and film thickness, h, over the spectral range of 340–1,600 nm. The laser irradiation tests were carried out using a Q-tuned Nd:YAG laser, which provided a nearly Gaussian-type pulse beam at 1,064-nm wavelength. A detailed description of the optical setup was given elsewhere [36]. The maximum output energy at 1,064 nm was 800 mJ, the pulse duration was 3 ns, and the laser spot on the tested film was 1 mm^2. The laser damage resistance of films was measured using the R/1 testing mode. And the film damages were estimated from the visual inspection of the plasma flash and detected in situ with a Normarski interferential contrast microscope.

3 Results and discussion

3.1 Stability and microstructure of ZrO_2-based sols

As mentioned above, for application in HR mirrors, ZrO_2 films must obtain their properties directly from the sol–gel deposition, which should base on precursor sols with both sufficient hydrolysis-condensation of zirconium precursors and proper stability. To this end, the sol–gel processing parameters, especially the system composition, should be properly selected.

Thus, before the synthesis of PVP/ZrO_2-based hybrid materials, we prepared ZrO_2-based sols first in order to give a primary optimization on the system composition. Our experiments showed that both the stability and structure of ZrO_2-based colloidal system strongly depended on its composition, especially the chelating ratio, d. It is clear from Table 1 that, at the fixed $Zr(OPr)_4$ concentration, C, of 0.28 mol/L and hydrolysis ratio, r, of 2:1, only when the chelating ratio, d, exceeds 0.5:1, can a stable sol be obtained. Here, a stable sol refers to such a system that can maintain the transparent state and good fluidity after 20-day aging at 293 K. Obviously, from the viewpoint of sol stability, d can be selected in a wide range. For our specific application, however, it should be further confined. Figure 1 illustrates the $J(q)$ vs. q plots of the SAXS intensity of ZrO_2-based colloid samples prepared at different chelating ratio, d. For comparison, the scattering curve of the chelating solution is also displayed. Clearly, both the chelating solution and sols with d of 2:1–1:1 scatter X-rays very weakly, suggesting the absence of significant quantities of particles larger than 1 nm. As the chelating ratio, d, decreases to 0.8:1 or less, noticeable SAXS from the colloid system occurs and the scattering curves tend progressively to a typical power law dependence of $J(q)$ on q at the intermediate q region, indicating the emergence of a large number of detectable colloidal particles and the formation of fractal clusters. Such a gradual change in the SAXS intensity provides a clear overview on the structural change of the colloidal system, and can be essentially associated with the different degree to which the controlled hydrolysis-condensation can reach.

Although there has not been a generally accepted mechanism on the chelation between DEA and zirconium alkoxides, based on the coordination chemistry of zirconium and structural characteristics of DEA molecules, the

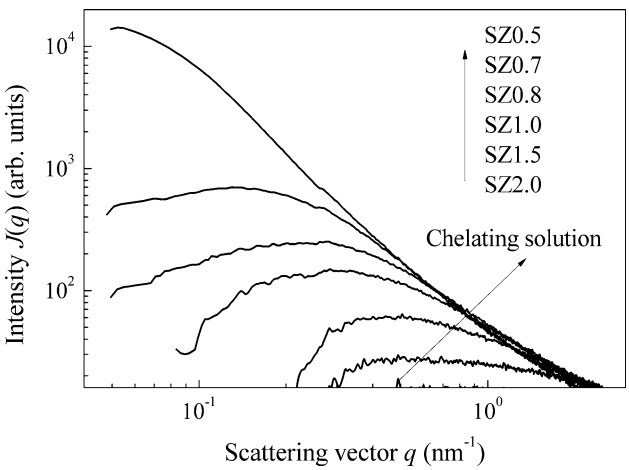

Fig. 1 $J(q)$ vs. q plots of the SAXS intensity for ZrO_2-based colloidal samples prepared at different chelating ratio, d

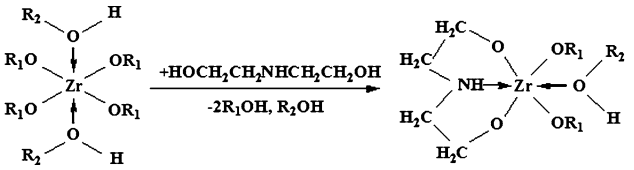

Fig. 2 The possible chelating reaction occurred between $Zr(OPr)_4$ and DEA

possible chelating reaction in our case can be expressed by Fig. 2, where R_1 and R_2 denote propyl (C_3H_7) and ethyl (C_2H_5), respectively [37]. Undoubtedly, we present here just a general description of the complex chelating reactions. With different chelating ratio, d, various new chelating species may come into being, endowing the colloidal system with different stabilities and microstructure.

Based on such a chelating mechanism, a detailed correlation between the SAXS intensity, structure of the colloidal systems, and reaction extent of the controlled hydrolysis-condensation can be described as follows. In Fig. 1, the negligible scatterings from both the chelating solution and sols with high chelating ratio, d, indicate that zirconium atoms mainly exist in the form of soluble chelating intermediates due to the strong chelation between $Zr(OPr)_4$ and DEA. As d decreases, the chelating species consequentially exhibit more propoxyl groups available for the nucleophilic substitution by H_2O molecules, and hydrolysis-condensation becomes predominant in the reaction system. The increasing predominance of hydrolysis-condensation not only gives rise to a gradual increase in the size and number of the colloidal particles, but promotes the interconnection between particles to form the fractal clusters, which explains the fact that the scattering curves tend progressively to a power law dependence of $J(q)$ on q at the intermediate q region [34, 35]. The gradual increase in the mean diameter of the colloidal particles has been confirmed by both the SAXS and DLS analysis results, as shown in Table 1.

Considering both the sufficient hydrolysis-condensation of zirconium alkoxides and proper sol stability, the chelating ratio, d was selected as 0.6:1–0.7:1.

3.2 Microstructure of PVP/ZrO_2-based hybrid sols

Figure 3 displays the SAXS curves of the hybrid precursor sols samples that were directly used for film deposition. It is noticeable that both ZrO_2-based and PVP/ZrO_2-based sols scatter X-ray very similarly, implying no significant changes in size, amount, and fractal characteristics of colloidal particles with the incorporation of a certain amount of PVP. A typical particle size distribution curve is shown by the inset in Fig. 3. The mean particle diameter, $D_{m,\mathrm{SAXS}}$, is collected in Table 1. For all the sols, The

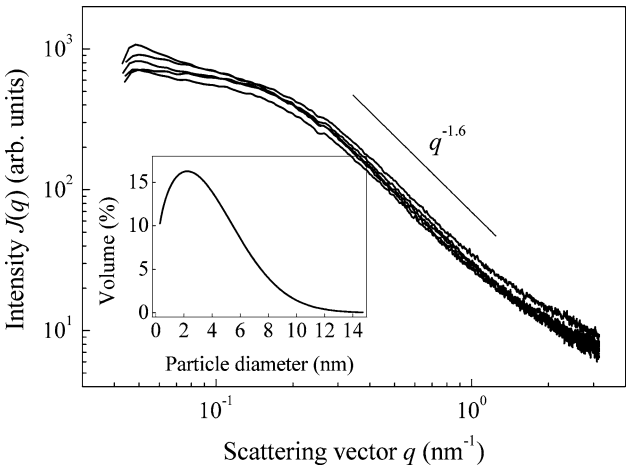

Fig. 3 $J(q)$ vs. q plots of the SAXS intensity for PVP/ZrO_2-based hybrid sols and a typical particle size distribution curve (inset)

SAXS analysis gives similar $D_{m,\mathrm{SAXS}}$ of 3.8–4.0 nm. Besides, all the scattering curves present a clear power law region with an exponent of −1.6 and a q-range from about 0.3 to 1.0 nm^{-1}. This suggests that the interconnection between the colloidal particles produces mass fractal clusters with the fractal dimension of about 2.6 [34, 35].

The DLS characteristics of these sols were also examined. The particle size distribution calculated from the DLS analysis shows that the vast majority of the scattering particles possess a hydrodynamic diameter, $D_{h,\ \mathrm{DLS}}$, in the range of 6–7 nm, as shown in Table 1. Most samples also contain a small fraction of 20–30-nm particles, which make up <5% of the solid weight. Moreover, data measured independently at the two angles gave very similar size distributions, lending weight to the DLS analysis.

The small discrepancy in the average particle "size" determined by the SAXS and DLS techniques is due to the presence of the interfacial layer necessary to stabilize the sol state. The interfacial layer is included in the hydrodynamic diameter, $D_{h,\ \mathrm{DLS}}$ (derived from DLS analysis), but has X-ray scattering characteristics very similar to those of the surrounding ethanol matrix and thus is not detected by SAXS.

Both the SAXS and DLS analyses suggest that the incorporation of a proper amount of PVP cannot have considerable influence on the microstructure of ZrO_2-based colloidal systems. This is completely different from the results of the previous studies on PVP-doped SiO_2, $BaTiO_3$, PZT, or $BaBi_4Ti_4O_{15}$ system, which indicated that the incorporation of PVP could have remarkable effect on the particle size distribution of the colloidal system [38–40]. The negligible PVP effect, in our case, is probably due to the presence of the chelating reactions that are particular to our ZrO_2-based systems. It can be predicted that, in the final sols, there must be a certain amount of

unhydrolyzed chelating ligands due to the chelate, electronic, and steric hindrance effects, which become anchored to zirconium oxo-polymeric backbone and form O/I networks. The presence of DEA segments in the inorganic networks may considerably modify the property, especially the surface property, of colloidal particles by declining both the number and activity of the surface hydroxyls, hence concealing and weakening the effect of PVP from the following two aspects. Firstly, the presence of the unhydrolyzed DEA segments may restrict the growth and interaction of colloidal particles, which is similar to the protective effect of PVP polymers in preventing the formation of large agglomerates by enveloping the particles with their polymer chains [39, 40], but in a more powerful way due to the direct and strong bonding of DEA with zirconium atoms. This makes the influence of PVP unable to be expressed and detected, even though its presence is undeniable. Secondly, the declined activity of surface hydroxyls may, to some extent, weaken the hybridization between PVP chains and ZrO_2-based particles, which has been known as the class I hybridization formed by hydrogen bond between the surface hydroxyls of ZrO_2 particles and the electronegative oxygen atoms of inner amide in PVP [20]. A schematic representation of the effect of DEA segments on the interaction between PVP and ZrO_2-based particles is shown in Fig. 4. Such a conjecture is confirmed by our FTIR analysis and will be discussed later.

From the above analysis, it can be conjectured that, in our case, the incorporation of PVP must have no considerable influence on the nucleation and growth of ZrO_2-based particles, and the PVP chains may just uniformly disperse in the hybrid sols through the weakened hydrogen bonding with ZrO_2-based particles as well as spatial interconnection with ZrO_2-based networks. It is worth noting, however, even the considerable surface modification of the DEA segments is taken into account, the weak alkaline synthetic environment (pH value of about 8) can still produce ZrO_2-based particles with enough active surface hydroxyls to connect each other to form networks and to bond with PVP chains. Moreover, the in situ hybridization route also offers a deep complecting between the PVP chains and ZrO_2-based networks. Therefore, the combined effect of the weak alkaline synthetic system and the in situ hybridization route keeps PVP chains deeply anchored to the ZrO_2-based polymeric backbones in the final hybrid sols and then films.

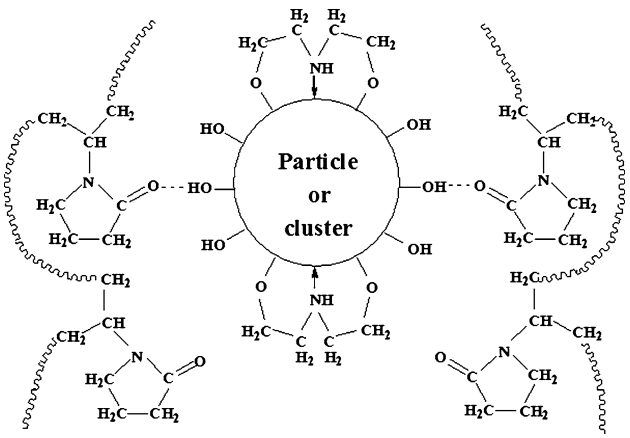

Fig. 4 A schematic presentation of the effect of DEA segments on the interaction between PVP and ZrO_2-based particles

3.3 FTIR and AFM analyses of PVP/ZrO_2-based films

The FTIR spectra of all the hybrid samples are displayed in Fig. 5. The Zr–O–Zr and Zr–O stretching vibrations of the inorganic segments are observed from the strong, broad absorption bands around 460 and 615 cm^{-1} [41]. The absorption bands at 934 and 1,098 cm^{-1}, with Zr–OC stretching at 934 cm^{-1} and ZrO–C stretching at 1,098 cm^{-1}, show evidence of the unhydrolyzed DEA ligands directly bonding with zirconium atoms [28, 30, 41]. The typical stretching vibration bands of C–N and C=O in PVP molecules are observed at 1,290 and 1,660 cm^{-1}, respectively [20]. These two bands gradually increase in intensity with the increase of the designed PVP content, indicating that an increasing amount of PVP has been incorporated into the films. Besides, all the spectra exhibit two absorption bands at 1,578 and 1,630 cm^{-1}, which might be derived from the deformation vibration of H_2O molecules that was adsorbed from the atmosphere during the FTIR measurement.

Figure 6 shows the typical AFM images of the hybrid sample, FZP15. The average roughness, R_a, and mean square roughness, R_q, for all the films are collected in Table 2. The mean square roughness ranges from 1.07 to 1.54 nm, suggesting the excellent surface planarity of the films derived from the small particles size of our precursor

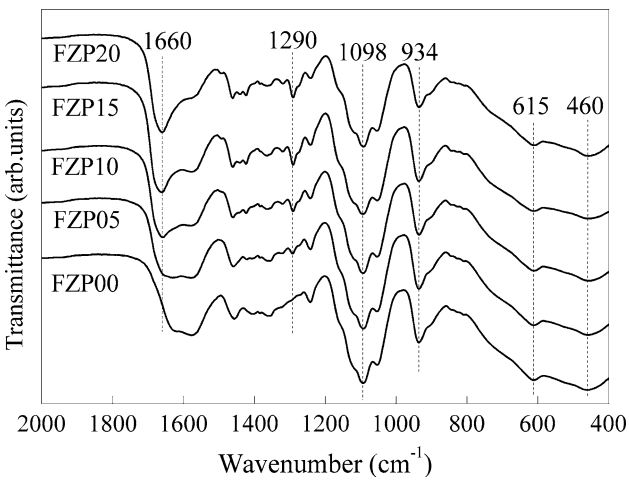

Fig. 5 FTIR spectra of PVP/ZrO_2-based hybrid films

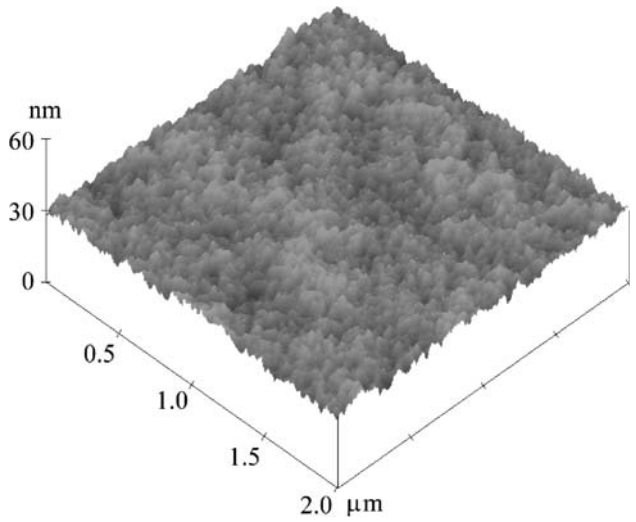

Fig. 6 The typical AFM diagrams of the hybrid film sample, FZP15

Table 2 Structural and optical properties of PVP/ZrO_2-based high-index and SiO_2 low-index layers

Sample	R_a (nm)	R_q (nm)	λ_0 (nm)	$T_{\lambda 0}$ (%)	n (at 1,064 nm)	h (nm)
FZP00	0.88	1.07	1,060	89.9	1.615	164.8
FZP05	0.92	1.15	1,065	90.0	1.612	165.6
FZP10	1.04	1.22	1,070	90.1	1.610	166.5
FZP15	1.10	1.38	1,065	90.1	1.607	166.1
FZP20	1.23	1.54	1,075	90.2	1.604	167.1
SiO_2 film	0.48	1.16	1,065	96.0	1.228	216.5
Errors	±0.02	±0.02	±5	±0.2	±0.002	±0.5

R_a and R_q are the average roughness and mean square roughness of the film surface derived from AFM analysis. λ_0 and $T_{\lambda 0}$ denote the central wavelength and the corresponding transmittance of determined from the UV/Vis/NIR transmission spectra. n and h denote the refractive index and film thickness measured by the FilmTek^{TM}3000 thin-film metrology system

sols. Low roughness reduces the surface scattering loss and promises good optical properties.

3.4 Optical properties of PVP/ZrO_2-based films

The UV/Vis/NIR transmission spectra (not shown here) of all ZrO_2-PVP films exhibit the typical reflective characteristics of the high-index materials with the central wavelength, λ_0, around 1,064 nm and minimum transmittance, $T_{\lambda 0}$, of about 90%, as summarized in Table 2. The dispersion curves of the refractive indices, $n(\lambda)$, and extinction coefficients, $k(\lambda)$, in the spectral range of 340–1,600 nm are displayed in Fig. 7. As expected, our ZrO_2 xerogel films show a high refractive index of about 1.63 (at 632.8 nm), larger than the values of 1.57–1.59 (at 632.8 nm) reported in current literatures for the sol–gel

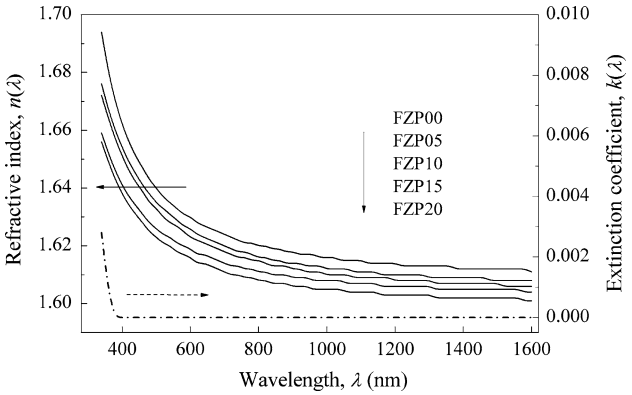

Fig. 7 The dispersion curves of the refractive indices, $n(\lambda)$, and extinction coefficients, $k(\lambda)$, of PVP/ZrO_2-based films in the spectral range of 340–1,600 nm

derived ZrO_2 films [8, 42, 43]. This must benefit from the comparatively sufficient hydrolysis and condensation of zirconium precursors owing to the proper selection of the system composition assisted by the light scattering techniques. However, such a value is still much lower than that of the bulk crystalline ZrO_2 (about 2.17 [43]). This must be an inevitable consequence of the presence of certain amount of DEA ligands directly bonding to zirconium atoms and the incomplete oxolation of hydroxyls in the xerogel films (as demonstrated by the FTIR analysis). And undoubtedly, the amorphous phase composition and the porous network structure of the sol–gel derived films must be also responsible for the index discrepancy between the as-deposited films and that of the crystalline bulk materials. Moreover, compared with sample FZP00, the incorporation of PVP only gives rise to a slight change in the refractive index, in consistent with our previous conjecture that the PVP chains are just uniformly dispersed in the hybrid sols and cannot have considerable influence on the controlled hydrolysis-condensation of $Zr(OPr)_4$. And the uniformly dispersed PVP chains in the hybrid sols and then films, which have a relatively lower index than ZrO_2-based backbones, must account for the slight decrease in refractive index of the films. At 1,064 nm, the refractive index, n decreases from 1.615 for sample FZP00 to 1.604 for FZP20, as shown in Table 2. Besides refractive indices, the extinction coefficients, $k(\lambda)$, and thickness, h, of the films were obtained simultaneously. The k values are almost zero for all the studied films in the spectral range of 380–1,600 nm, indicating negligible absorption of films in the visible and near infrared spectral region. The film thickness ranges from 164.8 to 167.1 nm, as shown in Table 2.

3.5 Laser irradiation test on PVP/ZrO_2-based films

The laser-irradiation experiments were performed using $R/1$ mode. For each sample, the irradiation test was carried out at

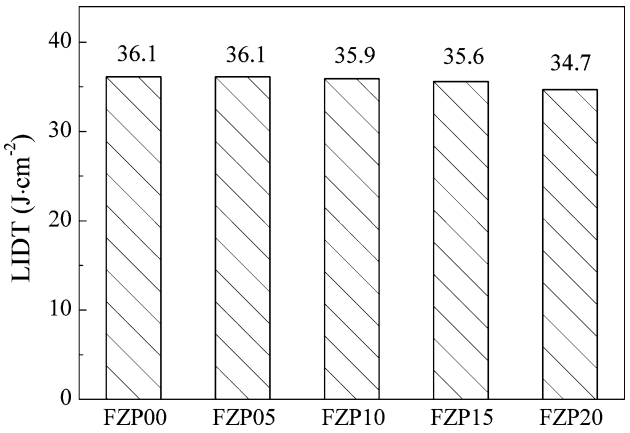

Fig. 8 The LIDT values of PVP/ZrO_2-based films (at 1,064 nm, 3 ns pulse duration and *R*/1 testing mode)

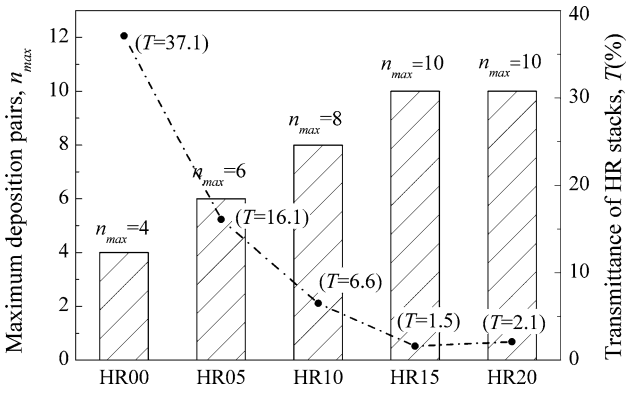

Fig. 9 The structural and optical properties of HR mirrors. (n_{max} and *T* denote the maximum deposition pairs and the minimum transmittance of the HR mirrors, respectively)

20 different sites that were arranged in a 4 × 5 array to obtain the representative laser-induced damage threshold (LIDT) of films. The LIDT values listed in Fig. 8 correspond to the highest energy at which no damage occurred. As expected, our PVP/ZrO_2-based films exhibit high LIDT values of 34.7–36.1 J/cm^2 (at 1,064 nm, 3 ns pulse duration), larger than the reported value of 18.8 J/cm^2 (at 1,064 nm, 12 ns pulse duration) for ZrO_2 films deposited by the electron beam evaporation method [16], and matching the reported values of 45–50 J/cm^2 (at 1,064 nm, 5–7 ns pulse duration) for the sol–gel derived ZrO_2 films [3–6, 44]. The high LIDT of the films must be related to their structural advantages such as homogeneity, nearly free of defects and impurities, as well as the low internal stresses. Additionally, with the incorporation of PVP, no significant changes in the LIDT can be observed, which might occur as another consequence of the negligible influence of PVP on the controlled hydrolysis-condensation of $Zr(OPr)_4$.

3.6 Preparation and properties of the HR mirrors

Hereinbefore, we have given a detailed investigation on PVP/ZrO_2-based high-index layers. The preparation of the HR mirrors, Substrate//(PVP/ZrO_2-based)//[SiO_2//(PVP/ZrO_2-based)]^*n*, involves an alternate deposition of PVP/ZrO_2-based and SiO_2 layers. For a better understanding of the optical performance of the HR mirrors, we present here a brief summary on the characterization results of our SiO_2 sol and the low-index film. As shown in Table 1, SiO_2 sol consists of colloidal particle with the mean hydrodynamic diameter of 12.3 nm and standard deviation of 2.1 nm, and its viscosity is 1.82 cP (at the spinning rate of 100 rpm). The thickness of our SiO_2 film is 216.5 nm and it exhibits a refractive index of 1.228 at 1,064 nm, as collected in Table 2.

Using different PVP/ZrO_2-based films but identical SiO_2 film as the high- and low-index layers, a series of HR mirrors were prepared. Our experiment showed that the incorporation of PVP could remarkably influence the stress compatibility between PVP/ZrO_2-based and SiO_2 layers, and thus determine the maximum deposition pairs, n_{max}, and the minimum transmittance, *T*, of the HR mirrors, as shown in Fig. 9. Clearly, with the increase of PVP content, the maximum deposition pairs, n_{max}, increases, implying that the incorporation of PVP can enhance the stress compatibility between different layers by energy relaxation through their flexible polymer chains. As the mass fraction of PVP reaches 15–20%, a perfect stress match between PVP/ZrO_2-based and SiO_2 layers can be achieved, which enables the successful deposition of 21-layer, nearly full-reflection mirrors with the minimum transmittance of 1.5–2.1% (at 1,064 nm). The typical transmission spectra of the HR mirrors are shown in Fig. 10. In addition, our sol–gel derived HR mirrors exhibit high LIDTs of 24.2–26.9 J/cm^2 (at 1,064 nm, *R*/1 mode, and 3 ns pulse duration), in compliance with the requirements of high-power

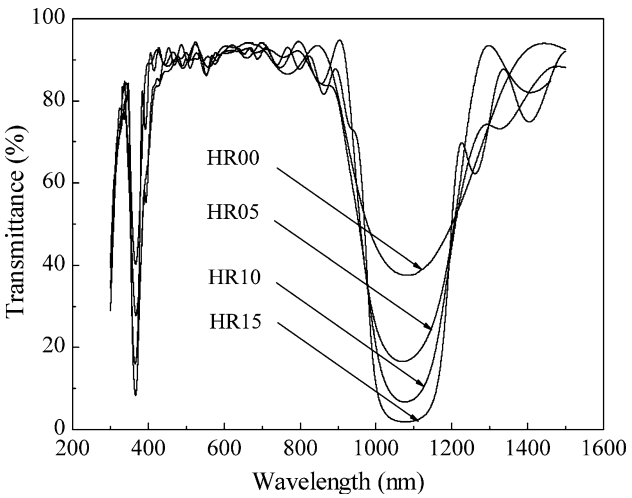

Fig. 10 The typical transmission spectrum of the HR mirrors

lasers (about 18 J/cm^2 at 1,064 nm wavelength, *R*/1 mode and 3 ns pulse duration).

4 Conclusion

In this study, PVP/ZrO_2-based hybrid films were prepared using the sol–gel route followed by spin-coating technique. Due to the structural advantages derived from both the sol–gel route and the O/I hybrid materials, the prepared films exhibit good optical properties and high laser induced damage resistance. Light scattering studies on the precursor sols demonstrate that, in the hybrid system, the chelating reaction between DEA and $Zr(OPr)_4$ may considerably conceal and weaken the effect of PVP on the nucleation and growth of ZrO_2-based particles. Therefore, the incorporation of PVP only leads to slight decreases in the refractive index and LIDT of the films. However, at the small expense of the refractive index and LIDT of the high-index layers, the addition of PVP can easily alleviate the stress incompatibility between PVP/ZrO_2-based and SiO_2 layers, and then facilitates the deposition of the multi-layer HR mirrors.

Acknowledgements The authors are very grateful to Dr. Zhihong Li and Zhonghua Wu (National Synchrotron Radiation Laboratory, Institute of High Energy Physics, Chinese Academy of Sciences) for their help in SAXS experiments, to the Scientific Computing International Company for performing some of the film characterization. The financial support from the National Key Native Science Foundation, China (Grant Number 20133040) is also gratefully acknowledged.

References

1. Thomas IM (1987) Appl Optics 26:4688
2. Floch HG, Priotton JJ, Thomas IM (1990) SPIE 1328:307
3. Thomas IM (1994) SPIE 2288:50
4. McInnes HA, Andrew JE, Bazin NJ, Morris AJ, Porter KJ (1997) SPIE 3244:500
5. Belleville Ph, Bonnin C, Lavastre É, Pégon Ph, Rorato Y (2000) SPIE 4347:588
6. McInnes HA, Andrew JE, Bazin NJ, Morris AJ (2000) SPIE 3902:215
7. Zhang QY, Shen J, Wang J, Wu GM, Chen LY (2000) Int J Inorg Mater 2:319
8. Grosso D, Seromon PA (2000) Thin Solid Films 368:116
9. Pégon P, Germain C, Rorato Y, Belleville Ph, Lavastre E (2004) SPIE 5250:170
10. Belleville Ph, Prené Ph, Bonnin C, Beaurain L, Montouillout Y, Lavastre É (2004) SPIE 5250:196
11. Zhao Y, Tang ZS, Shao J, Fan Z (2004) SPIE 5273:23
12. Higgins TV (1994) Laser Focus World 9:61
13. Reichling M, Bodemann A, Kaiser N (1998) Thin Solid Films 320:264
14. Zhao YA, Gao WD, Shao JD, Fan ZX (2004) Appl Surf Sci 227:275
15. Thomas IM (1986) Appl Optics 25:1481
16. Tian GL, Huang JB, Wang T, He HB, Shao JD (2005) Appl Surf Sci 239:201
17. Zhang DW, Fan SH, Zhao YA, Gao WD, Shao JD, Fan RY, Wang YJ, Fan ZX (2005) Appl Surf Sci 243:232
18. Zhao YA, Wang T, Zhang DP, Fan SH, Shao JD, Fan ZX (2005) Appl Surf Sci 239:171
19. Zhu XL, Shi L, Chan J, Wang J, Ye C, Lo D (2005) Opt Commun 251:322
20. Egger P, Sorarù GD, Diré S (2004) J Eur Ceram Soc 24:1371
21. Lenormand P, Caravaca D, Laberty-Robert C, Ansart F (2005) J Eur Ceram Soc 25:2643
22. Egger P, Sorarù GD, Ceccato R, Diré S (2005) J Eur Ceram Soc 25:2647
23. Stöber W, Fink A, Bohn E (1968) J Colloid Interface Sci 26:62
24. Xu Y, Liu RL, Wu D, Sun YH, Gao HC, Deng F (2005) J Non-Cryst Solids 351:2403
25. Kathryn GS, Jeffrey SL (1994) Chem Mater 6:890
26. Ehrhart G, Capoen B, Robbe O, Boy Ph, Turrell S, Bouazaoui M (2006) Thin Solid Films 496:227
27. Ohya T, Kabata M, Ban T, Ohya Y, Takahashi Y (2002) J Sol–Gel Sci Technol 25:43
28. Méndez-Vivar J, Mendoze-Serna R, Valdez-Castro L (2001) J Non-Cryst Solids 288:200
29. Pan M, Liu JR, Lu MK, Xu D, Yuan DR, Chen DR, Yang P, Yang ZH (2001) Thermochim Acta 376:77
30. Zhao JP, Fan WH, Wu D, Sun YH (2000) J Non-Cryst Solids 261:15
31. Guinebretière R, Soulestin B, Dauger A (1998) Thin Solid Films 319:197
32. Guinebretière R, Dauger A, Masson O, Soulestin B (1999) Phil Mag A 79:1517
33. Xu Y, Wu D, Sun YH, Li ZH, Dong BZ, Wu ZH (2005) Acta Phys Sin 54:2814
34. Keefer KD, Schaefer DW (1986) Phys Rev Lett 56:2376
35. McMahon PJ, Moss SD (2002) J Appl Cryst 32:956
36. Xu Y, Zhang L, Wu D, Sun YH, Huang ZX, Jiang XD, Wei XF, Li ZH, Dong BZ, Wu ZH (2005) J Opt Soc Am B 22:905
37. Brian LC, Vladimir LK, Charles JÓ (2004) Chem Rev 104:3893
38. Xu Y, Zhang B, Fan WH, Wu D, Sun YH (2003) Thin Solid Films 440:180
39. Kozuka H, Takenaka S, Tokita H, Okubayashi M (2004) J Eur Ceram Soc 24:1585
40. Linardos S, Zhang Q, Alcock JR (2006) J Eur Ceram Soc 26:117
41. Sorek Y, Zevin M, Reisfeld R, Hurvits T, Ruschin S (1997) Chem Mater 9:670
42. Cueto LF, Sánchez E, Torres-Martínez LM, Hirata GA (2005) Mater Charact 55:263
43. Díaz-Parralejo A, Caruso R, Ortiz AL, Guiberteau F (2004) Thin Solid Films 458:92
44. Ferrara MC, Perrone MR, Protopapa ML, Sancho-Parramon J, Bosch S, Mazzarelli S (2004) SPIE 5250:537